

Letters

A Five-Switch Bridge Based Reconfigurable *LLC* Converter for Deeply Depleted PEV Charging Applications

Cheng Li, *Student Member, IEEE*, Haoyu Wang , *Member, IEEE*, and Ming Shang 

Abstract—This letter presents a reconfigurable dual *LLC* converter based on a five-switch bridge to charge the deeply depleted plug-in electric vehicle onboard battery packs. Due to the reconfiguration of the primary-side switch network, two resonant tanks could operate in integrated half-bridge, half-bridge, hybrid-bridge, and full-bridge modes. Thus, four operation modes are derived, with their normalized voltage gains scaled to 1:2:3:4, respectively. Those four modes enable a squeezed switching frequency span, which is close to the resonant frequency. Therefore, the efficiency performance over an ultra-wide output voltage range can be optimized. Zero-voltage-switching can be realized in all power MOSFETs over the entire load range. The operating principles, voltage gains analysis are briefed. A 1.1-kW-rated prototype converting the 390-V input to 100–420 V output, is designed and tested to validate the proof of concept. A total of 97.64% of peak efficiency and good efficiency over the full charging range is reported.

Index Terms—Circuit reconfiguration, five-switch bridge, *LLC*, plug-in electric vehicle (PEV) charging.

I. INTRODUCTION

THE Li-ion battery is widely used in plug-in electric vehicles (PEVs) as the main energy storage unit. The typical charging profile of a deeply depleted Li-ion battery cell is plotted in Fig. 1 [1]. As indicated, the cell voltage exhibits a wide voltage range (1–4.2 V) during the whole charging process. In high-power PEV battery packs, the cell voltage range is mapped to an ultra-wide pack voltage range (typically 100–420 V). This brings challenges to the optimal design of the dc/dc stage of the PEV onboard charger.

Frequency modulated *LLC* resonant converter is considered as a suitable candidate, mainly due to its attractive features

Manuscript received September 18, 2018; accepted October 3, 2018. Date of publication October 8, 2018; date of current version March 29, 2019. This work was supported in part by the National Natural Science Foundation of China under Grant 51607113 and in part by the Shanghai Sailing Program under Grant 16YF1407600. (*Corresponding author: Haoyu Wang.*)

C. Li is with the School of Information Science & Technology, ShanghaiTech University, Shanghai 201210, China, and also with the Chinese Academy of Sciences, Shanghai Institute of Microsystem and Information Technology, University of Chinese Academy of Sciences, Shanghai 200050, China (e-mail:

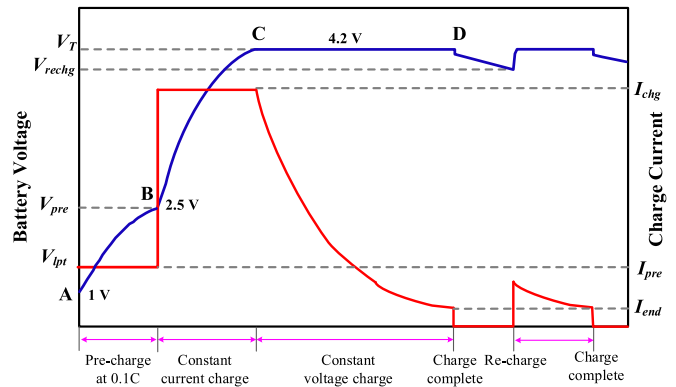


Fig. 1. Charging profile of a deeply depleted Li-ion battery cell.

such as soft switching, galvanic isolation, low EMI, and low components count [2]. However, to achieve such a wide voltage range, an ultra-wide switching frequency (f_s) range is required. This might lead to efficiency reduction, soft-switching loss, and degraded voltage regulation [3].

To narrow down the f_s range, many control schemes have been studied [4]–[6]. A variable-frequency plus phase-shift control is proposed in [4]. With phase-shift control at resonant frequency (f_r), the frequency range ($f_s > f_r$) is avoided and a low step-down voltage gain is achieved. In [5], a two-stage onboard charger with variable dc-link voltage is introduced. The voltage modulation range is extended, and f_s range is squeezed. However, the dc-link voltage range is limited by the front-end ac/dc stage.

Voltage modulation on the secondary side can also extend the output range with a narrow frequency span. In [7], a semi-active variable-structure rectifier is proposed. The rectifier could operate in voltage-doubler and voltage-quadrupler modes. Thus, f_s range is narrowed down. Similarly, a secondary structure with reconfigurable type-4/5/6 voltage multiplier rectifier is proposed in [8]. A squeezed frequency span is achieved with modes switch.

Another feasible solution is to switch the operation on the primary side based on the output voltage range [9], [10]. In [9], an *LLC* resonant converter with two resonant tanks is proposed. Two resonant tanks' secondary sides are in series. On the primary side, two resonant tanks are in series in low voltage

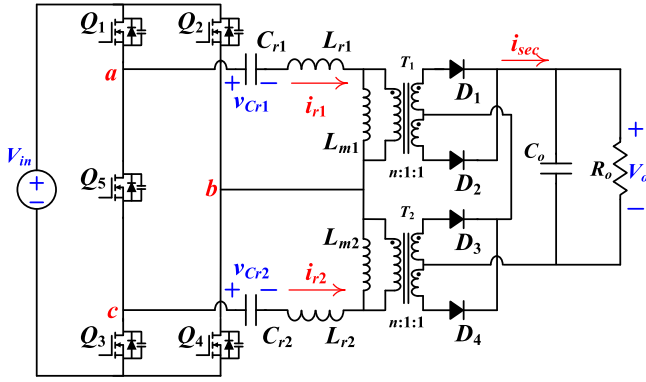


Fig. 2. Schematic of the proposed converter.

gain mode and in parallel in high voltage gain mode. Thus, the f_s range is squeezed. In [10], a modified *LLC* converter with adjustable turns ratio transformer is proposed. The turns ratio could be adjusted by a bidirectional switch. Thus, four operation modes with different voltage ranges can be realized. However, the device utilization rate is relatively low.

In this letter, a reconfigurable *LLC* converter based on a five-switch bridge on the primary side is proposed for deeply depleted PEV battery charging applications. Its advantages include the following.

- 1) Ultra-wide voltage range.
- 2) Squeezed f_s range close to f_r .
- 3) Full zero-voltage-switching (ZVS) over wide load range.
- 4) Reduced conduction loss with halved resonant current (i_r).
- 5) Simple structure and easy to extend.

II. PROPOSED CONVERTER AND OPERATING PRINCIPLES

Fig. 2 shows the schematic of the proposed *LLC* converter. The primary side is a reconfigurable bridge consists of five MOSFETs. Two *LLC* resonant tanks (RT1 and RT2) are connected with this five-switch bridge. It should be noted that the parameters including resonant inductances (L_r), resonant capacitances (C_r), magnetizing inductances (L_m), and transformer turns ratio (n) in those two resonant tanks are identical. On the secondary side, two center-tapped full wave rectifiers are in series. By configuring the primary-side MOSFETs in ON or OFF states, the inputs of the resonant tanks can be configured as full-bridge or half-bridge. Therefore, four combinations of switch patterns lead to four operation modes. The primary-side circuits of those four operation modes are plotted in Fig. 3.

Mode 1: In Mode 1, Q_3 is constantly ON while $Q_{2,4}$ are constantly OFF; Q_1 and Q_5 are driven complementarily with certain deadband. RT1 and RT2 are in series and integrated into one resonant tank. This integrated resonant tank operates in half-bridge mode and its input (v_{ac}) is a two-level (0 to V_{in}) square wave. v'_{ac} 's root-mean-square (RMS) value is $V_{in}/2$.

Mode 2: In Mode 2, $Q_{1,3}$ are constantly ON while Q_5 is constantly OFF; Q_2 and Q_4 are driven complementarily with certain deadband. Therefore, the inputs of RT1 and RT2 (v_{ab}

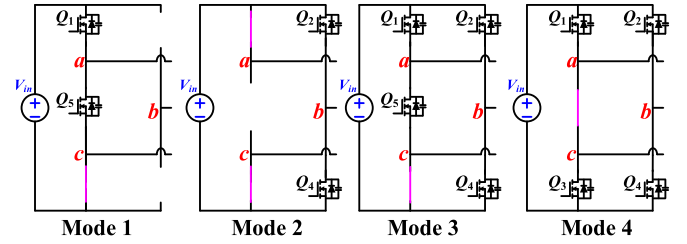


Fig. 3. Operation modes of the five-switch bridge.

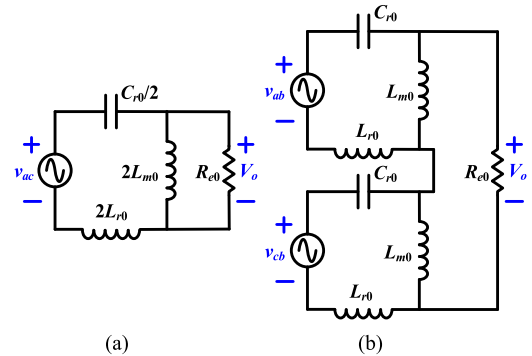


Fig. 4. Equivalent circuit model. (a) Mode 1. (b) Modes 2–4.

and v_{cb}) are both two-level square waves: 0 to V_{in} , and $-V_{in}$ to 0, respectively. This means both resonant tanks operate in half-bridge mode. v_{ab} and v'_{cb} 's RMS values are both $V_{in}/2$.

Mode 3: In Mode 3, Q_3 is constantly ON; $Q_{1,4}$ and $Q_{2,5}$ are driven complementarily with certain deadband. Therefore, v_{ab} and v_{cb} are both two-level square waves: $-V_{in}$ to V_{in} , and $-V_{in}$ to 0, respectively. This means RT1 operates in full-bridge mode while RT2 operates in half-bridge mode. v_{ab} and v'_{cb} 's RMS values are V_{in} and $V_{in}/2$, respectively. The power sharing between two resonant tanks are mismatched. Hence, equivalent load resistance (R_e) and equivalent output voltage in two resonant tanks are also mismatched.

Mode 4: In Mode 4, Q_5 is constantly ON; $Q_{1,4}$ and $Q_{2,3}$ are driven complementarily with certain deadband. Therefore, v_{ab} and v_{cb} are both two-level ($-V_{in}$ to V_{in}) square wave. Both resonant tanks operate in full-bridge mode. v_{ab} and v'_{cb} 's RMS values are both V_{in} .

III. VOLTAGE GAIN ANALYSIS

Using the first harmonic approximation (FHA) method, the equivalent sinusoidal circuit models of the proposed circuit in four modes are derived as shown in Fig. 4. R_{e0} is expressed

$$R_{e0} = \frac{8n^2}{\pi^2} R_o. \quad (1)$$

The key parameters of the resonant tanks in four modes are summarized in Table I. In Table I, $v_{g,rms}$ is the RMS value of the resonant tank's input voltage; Q is the quality factor; and m is the inductance ratio.

TABLE I
RESONANT PARAMETERS AND VOLTAGE GAIN

Mode	1		2		3		4	
Resonant tanks	1		2		2		2	
Q	Q_0	Q_0	Q_0	$1.5Q_0$	$0.75Q_0$	Q_0	Q_0	
m	m_0	m_0	m_0	m_0	m_0	m_0	m_0	
$v_{g,rms}$	$V_{in}/2$	$V_{in}/2$	$V_{in}/2$	$V_{in}/2$	V_{in}	V_{in}	V_{in}	
Gain	G_0		$2G_0$		$3G_0$		$4G_0$	

As indicated in Fig. 4(a), two resonant tanks are in series and construct an integrated resonant tank in Mode 1. The equivalent L_m and L_r are both doubled, the equivalent C_r is halved, and R_e is R_{e0} . Thus

$$Q_1 = \frac{\sqrt{2L_{r0}/(C_{r0}/2)}}{R_{e0}} = 2 \frac{\sqrt{L_{r0}/C_{r0}}}{R_{e0}} = Q_0 \quad (2)$$

$$m_1 = 2L_{m0}/(2L_{r0}) = L_{m0}/L_{r0} = m_0. \quad (3)$$

In Modes 2 and 4 [see Fig. 4(b)], both resonant tanks deliver equal power to the load. Thus, R_e for both resonant tanks is $R_{e0}/2$. Q and m in two resonant tanks are matched

$$Q_2 = Q_4 = \frac{\sqrt{L_{r0}/C_{r0}}}{R_{e0}/2} = Q_0 \quad (4)$$

$$m_2 = m_4 = L_{m0}/L_{r0} = m_0. \quad (5)$$

In Mode 3, the power sharing between two resonant tanks are mismatched. R_e of RT1 and RT2 are derived as $2R_{e0}/3$ and $R_{e0}/3$, respectively. It should be noted that Q is also mismatched while m is still matched

$$Q_{3.1} = \frac{\sqrt{L_{r0}/C_{r0}}}{2R_{e0}/3} = 0.75Q_0 \quad (6)$$

$$Q_{3.2} = \frac{\sqrt{L_{r0}/C_{r0}}}{R_{e0}/3} = 1.5Q_0 \quad (7)$$

$$m_{3.1} = m_{3.2} = L_{m0}/L_{r0} = m_0. \quad (8)$$

According to FHA method and equivalent sinusoidal circuit models, the voltage gain of resonant tank G_{LLC} is derived

$$G_{LLC} = \frac{mf_n^2}{\sqrt{[(m+1)f_n^2 - 1]^2 + m^2Q^2f_n^2(f_n^2 - 1)^2}} \quad (9)$$

where f_n is the normalized switching frequency f_s/f_r .

As aforementioned, due to identical Q and m , G_{LLC} in modes 1, 2, and 4 are the same (G_{LLC0}). In Mode 3, $Q_{3.1}$ is smaller than Q_0 while $Q_{3.2}$ is larger than Q_0 . Accordingly, the relationships in between G_{LLC} in four modes are expressed

$$G_{LLC3.1} > G_{LLC1} = G_{LLC2} = G_{LLC4} = G_{LLC0} > G_{LLC3.2}. \quad (10)$$

However, the total G_{LLC} in Mode 3, ($G_{LLC3.1} + G_{LLC3.2}$), is approximately $2G_{LLC0}$. Hence, G_{LLC} in four modes is considered to be identical. The overall voltage gain is determined

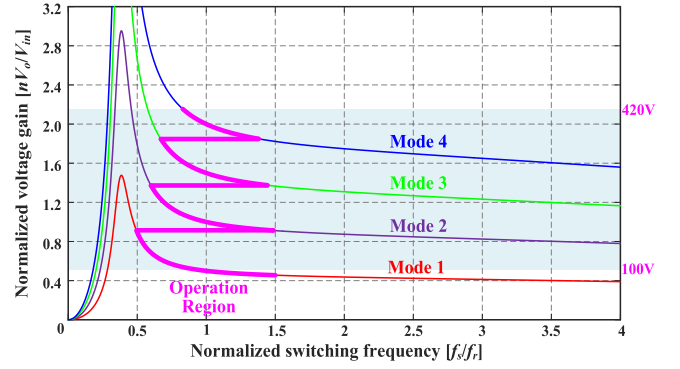


Fig. 5. Curves of normalized voltage gain versus normalized f_s .

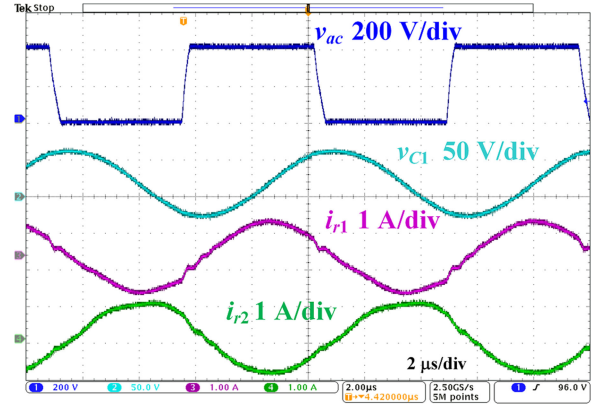


Fig. 6. Steady-state waveforms in Mode 1. $V_o = 100$ V. $P_o = 105$ W.

by $v_{g,rms}$ and the number of resonant tanks. In Mode 1, the voltage gain of the proposed converter is defined as G_0 . Thus, the voltage gains in mode 2, 3, and 4 are derived as $2G_0$, $3G_0$, and $4G_0$, respectively.

Correspondingly, the curves of normalized voltage gain versus normalized f_s in four modes are plotted in Fig. 5. As indicated, the mode transition facilitates both squeezed f_s range and extended voltage gain range. Thus, the efficiency performance over the wide output voltage range can be enhanced and the design complexity can be reduced.

IV. EXPERIMENTAL VERIFICATION

A 1.1-kW scale-down laboratory prototype for deeply depleted PEV charging is built to verify the effectiveness of the proposed converter. $V_{in} = 390$ V, $V_o = 100$ – 420 V. Q_1 – Q_5 : SCT3120, D_1 – D_4 : C3D10060A, transformers' turns ratio $n = 2:1$, $L_{m1} = L_{m2} = 382$ μ H, $L_{r1} = L_{r2} = 62$ μ H, $C_{r1} = C_{r2} = 32$ nF, $f_r = 100$ kHz, and f_s range is 50–150 kHz. At precharging stage, the charging current (I_o) is 1.05 A. At regular constant current (CC) charging stage, I_o is 2.62 A.

The steady-state waveforms in Mode 1 is captured in Fig. 6. As shown, v_{ac} is a two-level (0–390 V) square wave in half-bridge mode. i_{r1} equals $-i_{r2}$, which agrees well with the previous mode analysis. The steady-state waveforms in Mode 2 is captured in Fig. 7. As shown, v_{ab} and v_{cb} are both two-level

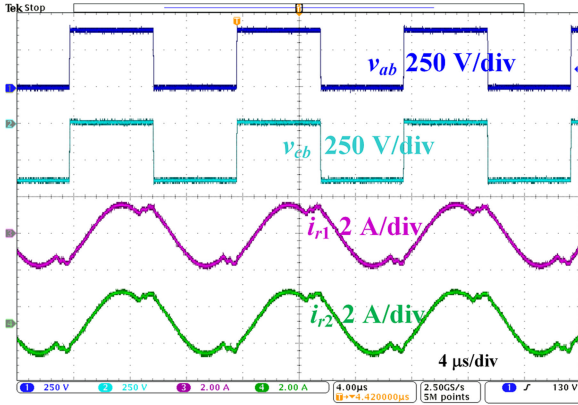


Fig. 7. Steady-state waveforms in Mode 2. $V_o = 230$ V. $P_o = 242$ W.

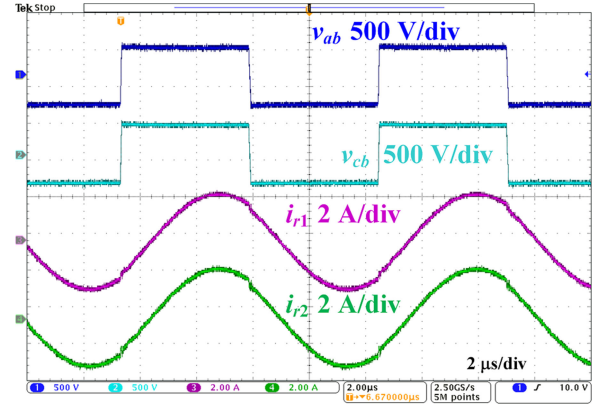


Fig. 9. Steady-state waveforms in Mode 4. $V_o = 417$ V. $P_o = 1.1$ kW.

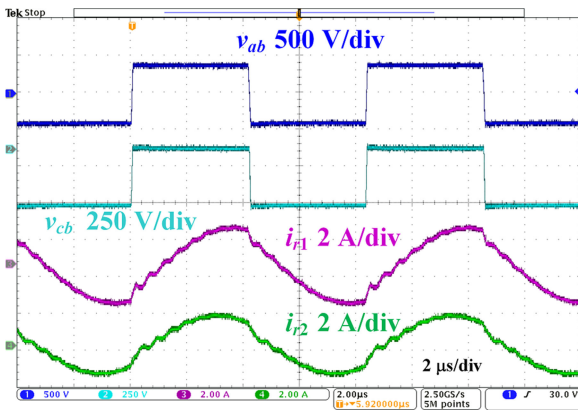


Fig. 8. Steady-state waveforms in Mode 3. $V_o = 300$ V. $P_o = 786$ W.

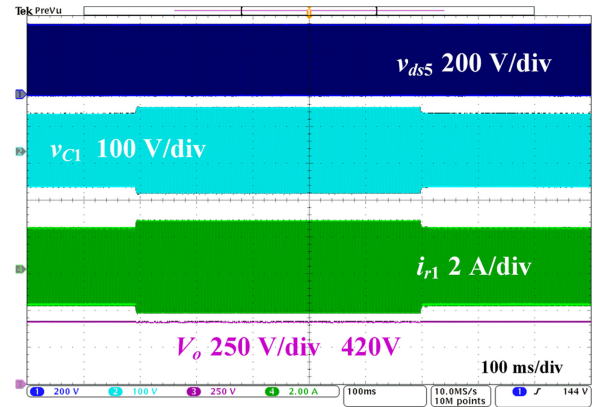


Fig. 10. Waveforms of voltage dynamic response in CV stage.

square waves (0 V to 390 V and -390 V to 0 V) in half-bridge mode. i_{r1} equals i_{r2} . This means that the power sharing between two resonant tanks are matched.

The steady-state waveforms in Mode 3 are captured in Fig. 8. As shown, v_{ab} is a two-level (-390 V to 390 V) square wave, while v_{cb} is a two-level (-390 V to 0 V) square wave. i_{r1} is larger than i_{r2} . This means RT1 delivers higher power than RT2. The main reason is that RT1 operates in full-bridge mode while RT2 operates in half-bridge mode. The steady-state waveforms in Mode 4 are captured in Fig. 9. As shown, v_{ab} and v_{cb} are both two-level (-390 V to 390 V) square waves in full-bridge mode. i_{r1} equals i_{r2} . This indicates that the power sharing between two resonant tanks are matched.

Fig. 10 demonstrates the dynamic response in constant voltage (CV) charging stage. The converter operates in Mode 4. V_o is well regulated to 420 V when load variation occurs. Fig. 11 demonstrates a smooth transition from Mode 1 to Mode 2 in precharging stage. In summary, the designed prototype demonstrates a robust dynamic response over the entire working range.

Fig. 12 provides the measured efficiency data in precharging and CC charging stages. As shown, when V_o increases, the operation mode changes from 1 to 4, accordingly. 190 V, 290 V, and 380 V mark the three mode transition points. Beyond those points, the latter mode demonstrates higher efficiency than the

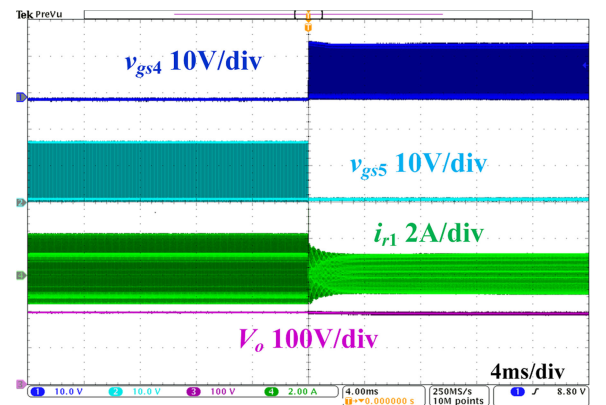
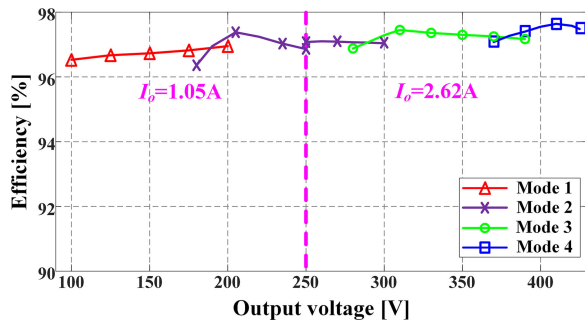
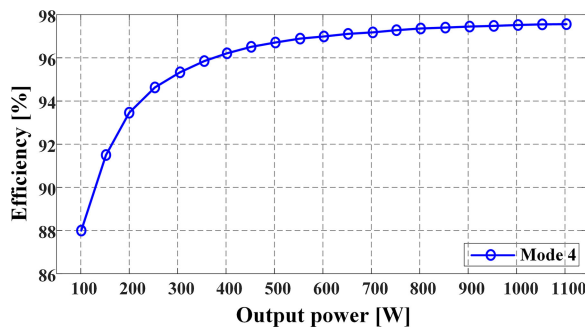


Fig. 11. Waveforms of mode transition from Mode 1 to Mode 2.

former mode. This is because the latter mode enables an f_s span closer to f_r . Thus, the circuit operation is more optimized. 250 V is the boundary between the precharging and CC charging stages where I_o steps from 1.05 A to 2.62 A. The converter demonstrates 97.64% peak efficiency and good overall efficiency.

Fig. 13 provides the measured efficiency data in the CV charging stage. As shown, the converter demonstrates 97.56% peak efficiency and good overall efficiency.

Fig. 12. Efficiency versus V_o in precharge and CC stage.Fig. 13. Efficiency versus P_o in CV stage, $V_o = 420$ V.

V. CONCLUSION

In this letter, a novel five-switch bridge based reconfigurable dual LLC converter is proposed for deeply depleted PEV charging applications. By adding only one extra MOSFET, the proposed converter could operate in four different modes with scaled voltage gain. Thus, it could provide an ultra-wide voltage range. With frequency modulation, f_s is constrained to be close to f_r over the entire output range. Thus, the efficiency performance

can be enhanced over the full load range. A 1.1-kW experimental prototype with 390-V input and 100–420 V output is built to verify the concept. The proposed converter is also suitable for other wide input/output voltage range applications and is compatible with other control methods and secondary rectifiers.

REFERENCES

- [1] H. Wang, S. Dusmez, and A. Khaligh, "A novel approach to design EV battery chargers using SEPIC PFC stage and optimal operating point tracking technique for LLC converter," in *Proc. IEEE Appl. Power Electron. Conf. Expo.*, 2014, pp. 1683–1689.
- [2] J. Deng, S. Li, S. Hu, C. C. Mi, and R. Ma, "Design methodology of LLC resonant converters for electric vehicle battery chargers," *IEEE Trans. Veh. Technol.*, vol. 63, no. 4, pp. 1581–1592, May 2014.
- [3] X. Sun, X. Li, Y. Shen, B. Wang, and X. Guo, "Dual-bridge LLC resonant converter with fixed-frequency PWM control for wide input applications," *IEEE Trans. Power Electron.*, vol. 32, no. 1, pp. 69–80, Jan. 2017.
- [4] H. Wu, X. Zhan, and Y. Xing, "Interleaved LLC resonant converter with hybrid rectifier and variable-frequency plus phase-shift control for wide output voltage range applications," *IEEE Trans. Power Electron.*, vol. 32, no. 6, pp. 4246–4257, Jun. 2017.
- [5] Z. Liu, B. Li, F. C. Lee, and Q. Li, "High-efficiency high-density critical mode rectifier/inverter for WBG-device-based on-board charger," *IEEE Trans. Ind. Electron.*, vol. 64, no. 11, pp. 9114–9123, Nov. 2017.
- [6] H. Wang, S. Dusmez, and A. Khaligh, "Maximum efficiency point tracking technique for LLC-Based PEV chargers through variable DC link control," *IEEE Trans. Ind. Electron.*, vol. 61, no. 11, pp. 6041–6049, Nov. 2014.
- [7] H. Wu, Y. Li, and Y. Xing, "LLC resonant converter with semiactive variable-structure rectifier (SA-VSR) for wide output voltage range application," *IEEE Trans. Power Electron.*, vol. 31, no. 5, pp. 3389–3394, May 2016.
- [8] M. Shang, H. Wang, and Q. Cao, "Reconfigurable LLC topology with squeezed frequency span for high-voltage bus-based photovoltaic systems," *IEEE Trans. Power Electron.*, vol. 33, no. 5, pp. 3688–3692, May 2018.
- [9] C.-E. Kim, J.-I. Baek, and J.-B. Lee, "High-efficiency single-stage LLC resonant converter for wide-input-voltage range," *IEEE Trans. Power Electron.*, vol. 33, no. 9, pp. 7832–7840, Sep. 2018.
- [10] H. Hu, X. Fang, F. Chen, Z. J. Shen, and I. Batarseh, "A modified high-efficiency LLC converter with two transformers for wide input-voltage range applications," *IEEE Trans. Power Electron.*, vol. 28, no. 4, pp. 1946–1960, Apr. 2013.